

Parameter cross-talk and leakage between spatially-separated unknowns in viscoelastic full waveform inversion

Scott Keating and Kris Innanen

ABSTRACT

Elastic and attenuative effects play a major role in the determination of wave amplitudes and phases observed at seismic sensors. Viscoelastic full waveform inversion (FWI) has the potential to recover much of the information content of measured seismic data by simultaneously accounting for these effects. However, viscoelastic FWI introduces a set of new challenges and open research questions, related to its use of frequency-variations and phase information. These impact our understanding of anelastic parameter resolution, especially the phenomenon of cross-talk. Cross-talk is typically characterized through analysis of the radiation patterns of point scatterers; however, the point scatterer model is not well suited to viscoelastic FWI, because: (1) attenuation introduces a significant potential for cross-talk between variables distant from one another in space, and (2) interpreting the effect of frequency and phase dependence on the radiation patterns of point scatterers is not straightforward. We present and examine a numerical approach to assessing viscoelastic cross-talk based on differences between various model residual quantities. With it, we observe strong cross-talk both between velocity and Q variables, and into density for a variety of acquisition geometries. Of particular note is our characterization of the tendency for Q variables to leak into elastic variables from which they are spatially separated. This type of cross-talk is not easily characterized through the use of radiation patterns.

INTRODUCTION

The goal of full waveform inversion (FWI) is to infer subsurface medium properties by maximizing the use of the information content of measured seismic data (Tarantola, 1984). This goal cannot be achieved in full, because approximate models of true wave propagation must be selected. However, the move from simple to more complex wave models, which better approximate true wave propagation, has historically led to improved recovery of useful, accurate information about the subsurface. Much of the information constraining subsurface elastic properties resides in the amplitude and phase of the observed waveform. Scalar-acoustic FWI cannot use such information effectively, because of its neglect of elastic and attenuative effects. Elastic, viscoacoustic, and, less frequently, viscoelastic FWI approaches have been developed to address this deficiency (e.g., Tarantola, 1986; Hicks and Pratt, 2001; Tromp et al., 2005; Malinowski et al., 2011; Kamei and Pratt, 2013; Métyvier et al., 2015; Plessix et al., 2016; Yang et al., 2016; Keating and Innanen, 2017). As in any multi-parameter FWI problem, inter-parameter trade-off, or ‘cross-talk’, is a major obstacle to the implementation of these approaches (e.g. Kamei and Pratt, 2013; Alkhalifah and Plessix, 2014; Pan et al., 2016). Cross-talk occurs when data residuals caused by an error in the estimate of one physical property are attributed to another, impeding convergence and potentially leading to mis-characterization in the inversion output. Strategies exist for cross-talk reduction, but to design these effectively it is important to understand the cross-talk process, i.e., to determine which properties leak in to one another, and to what extent.

The most commonly used tool for characterizing cross-talk is radiation pattern analysis (e.g. Tarantola, 1986; Moradi and Innanen, 2016; Oh and Alkhalifah, 2016; Kamath et al., 2017). Radiation patterns express the change in an incident wave-field after interacting with a point scatterer, typically in an otherwise homogeneous medium. These patterns change for different choices of model perturbation. Greater cross-talk is predicted when the radiation patterns of two variables vary proportionally within the range of scattering angles sensed in an experiment, because this behavior is suggestive that the two variables are not distinguished within the available data. Radiation patterns are not investigated for every variable in the inversion, as the number of these is very large. Instead, a representative radiation pattern for each parameter type is usually investigated, with the scattering point set at a fixed location.

In elastic and anisotropic FWI, radiation pattern analysis has proven effective in predicting cross-talk (e.g., Oh and Alkhalifah, 2016). Guided by analysis of the patterns to select inversion parameters with minimal overlap between different radiation patterns in the data, the extent of cross-talk in the inversion can be reduced. Scattering patterns do not, however, completely characterize cross-talk. They are not well suited to providing information about cross-talk between variables at different spatial locations, as two different scattering angles for variables at different locations may represent the same part of data space. They are limited to providing information about the gradient and do not naturally allow the effects of iteration to be characterized. Consideration of both the second-order aspects of the objective function (e.g., via the Hessian) and iteration are key to the successful implementation of multi-parameter FWI (e.g. Virieux and Operto, 2009; Operto et al., 2013); hence, scattering patterns do not provide for complete characterization of cross-talk.

Including attenuation in FWI complicates cross-talk in a way that makes radiation pattern analysis even less suitable. Cross-talk involving Q generally involves confusion between different parameters at different points in space. For instance, a density perturbation will exhibit cross-talk with a remote Q region obscuring it from the sources and receivers. Another complication is the frequency and phase dependence of these radiation patterns, which are key to distinguishing Q from velocity (Innanen and Weglein, 2007; Hak and Mulder, 2011; Keating and Innanen, 2017), but whose role in reducing cross-talk is more difficult to discern from a radiation pattern alone.

Cross-talk can also be analyzed by examining numerical FWI examples in which cross-talk occurs (e.g. Köhn et al., 2012; Operto et al., 2013). By comparing inversion results to a known true model, errors in the inversion process can be identified. Some of these errors can be attributed to cross-talk, but because confusion between parameters is not the only source of error in inversion, it can be difficult to accurately and confidently identify it. More accurate approaches to quantifying cross-talk can be designed by comparing inversion results of different ‘true’ models in synthetic tests, as in Kamei and Pratt (2013), or by investigating the Hessian matrix in a specific case, as in Pan et al. (2018).

Here we describe, and analyze with 2D frequency-domain simulations, an alternative approach to characterizing viscoelastic cross-talk, with some specially-designed numerical FWI tests on simple models. This approach allows cross-talk between parameters to be understood as a function of either or both incidence angle and/or frequency. It also naturally

accounts for the effect of iteration and spatial distribution on parameter resolution. If the models considered are suitably chosen, these results allow general conclusions to be drawn about the nature of cross-talk.

THEORY

The approach for viscoelastic FWI we investigate here largely follows the work of Keating et al. (2018). To simulate viscoelastic wave propagation, we solve by the finite difference method the 2D viscoelastic system described by Pratt (1990):

$$\omega^2 \rho u_x + \frac{\partial}{\partial x} \left[\tilde{\lambda} \left(\frac{\partial u_x}{\partial x} + \frac{\partial u_z}{\partial z} \right) + 2\tilde{\mu} \frac{\partial u_x}{\partial x} \right] + \frac{\partial}{\partial z} \left[\tilde{\mu} \left(\frac{\partial u_z}{\partial x} + \frac{\partial u_x}{\partial z} \right) \right] + f = 0 \quad (1)$$

and

$$\omega^2 \rho u_z + \frac{\partial}{\partial z} \left[\tilde{\lambda} \left(\frac{\partial u_x}{\partial x} + \frac{\partial u_z}{\partial z} \right) + 2\tilde{\mu} \frac{\partial u_z}{\partial z} \right] + \frac{\partial}{\partial x} \left[\tilde{\mu} \left(\frac{\partial u_z}{\partial x} + \frac{\partial u_x}{\partial z} \right) \right] + g = 0, \quad (2)$$

where ω is the angular frequency, ρ is the density, u_x and u_z are, respectively, the horizontal and vertical displacements, f and g are their respective source terms, and $\tilde{\lambda}$ and $\tilde{\mu}$ are the complex, frequency dependent Lamé parameters. Assuming a Kolsky-Futterman model of attenuation (Kolsky, 1956; Futterman, 1962), these are defined in terms of ρ , the P and S wave speeds, v_P and v_S , as well as the quality factors Q_P and Q_S , by

$$\tilde{\mu} = \left\{ v_S \left[1 + \frac{1}{Q_S} \left(\frac{1}{\pi} \log \frac{\omega}{\omega_0} + \frac{i}{2} \right) \right] \right\}^2 \rho \quad (3)$$

and

$$\tilde{\lambda} = \left\{ v_P \left[1 + \frac{1}{Q_P} \left(\frac{1}{\pi} \log \frac{\omega}{\omega_0} + \frac{i}{2} \right) \right] \right\}^2 \rho - 2\tilde{\mu}, \quad (4)$$

where ω_0 is a reference frequency. This system is solved using the finite difference equations set up by Pratt (1990), which take the form

$$\mathbf{S}\mathbf{u} = \mathbf{h}, \quad (5)$$

where \mathbf{u} is a vector containing u_x and u_z , \mathbf{h} is a vector containing f and g , and \mathbf{S} is a Helmholtz matrix containing the finite difference coefficients. The matrix \mathbf{S} applies a finite difference star to \mathbf{u} approximating the wave equation in equations 1 and 2. Perfectly matched layers (Berenger, 1994) are used to prevent reflections from the boundaries of the model.

Optimization and parameterization

The objective function for the FWI problem we consider here is

$$\Phi = \sum_{x_s, \omega} \frac{1}{2} \|\mathbf{d} - \mathbf{R}\mathbf{u}(\mathbf{m})\|_2^2, \quad (6)$$

where \mathbf{d} is a vector containing the measured data, \mathbf{R} is a matrix representing the receiver sampling of the wave-field, x_s represents the surface location of the source, ω is angular frequency, and \mathbf{m} is a vector containing subsurface model parameters. The gradient of this function with respect to \mathbf{m} was originally derived by Tarantola (1984), and was expressed in a simple, general form by Metivier et al. (2013) as

$$\frac{\partial \phi}{\partial \mathbf{m}} = \left\langle \frac{\partial S}{\partial \mathbf{m}} \mathbf{u}, \lambda \right\rangle, \quad (7)$$

where $\langle \cdot, \cdot \rangle$ represents an inner product, and λ satisfies

$$\mathbf{S}^\dagger \lambda = \mathbf{R}^T (\mathbf{R} \mathbf{u} - \mathbf{d}). \quad (8)$$

We formulate FWI in terms of five parameters, selected for their simplicity: $\alpha_1 \rho$, $\alpha_2 v_p^{-2}$, $\alpha_3 Q_p^{-1}$, $\alpha_4 v_s^{-2}$, and $\alpha_5 Q_s^{-1}$, where the α_n are scale terms introduced to improve conditioning. The elastic problem having been thoroughly investigated, our focus is on cross-talk involving the Q variables. The Q^{-1} parameterization is convenient because of its limited numerical range (in comparison to a Q parameterization).

A measure of cross-talk

Cross-talk can be defined as *the contribution to the inverted value of variable 1 occurring as the result of model error in variable 2*. Variable 1 can be different from variable 2 because they are distinct in spatial position or in type; each leads to behaviour that can be classified as cross-talk. Our focus is the case in which the variables are different in their parameter type (e.g., P-wave quality factor versus density). This definition of cross-talk covers an important class of behaviors which are undesirable in FWI, as they tend to slow convergence and give rise to misleading inversion results. The definition also lends itself to direct calculation in synthetic tests.

Let $\text{FWI}(\cdot)$ be an operator that contains a complete process of full waveform inversion; if \mathbf{d} are simulated data measurements generated from the model \mathbf{m} , and an initial model \mathbf{m}^0 is given, we reconstruct via FWI the estimate

$$\hat{\mathbf{m}} = \text{FWI}(\mathbf{d}(\mathbf{m}), \mathbf{m}^0). \quad (9)$$

The overall model residual at the outset of the process is $\mathbf{r} = \mathbf{m} - \mathbf{m}^0$. If the model grid has N rows (or depths) and M columns (or lateral positions), then \mathbf{m} is a $(5MN)$ -length vector

$$\mathbf{m} = \begin{bmatrix} \mathbf{m}_{vp} \\ \mathbf{m}_{vs} \\ \mathbf{m}_{qp} \\ \mathbf{m}_{qs} \\ \mathbf{m}_\rho \end{bmatrix}, \quad (10)$$

where each element (e.g., \mathbf{m}_{vp}) is an (MN) -length column vector containing the model

parameter values. Organized this way, the model residual is evidently

$$\mathbf{r} = \begin{bmatrix} \mathbf{m}_{vp} - \mathbf{m}_{vp}^0 \\ \mathbf{m}_{vs} - \mathbf{m}_{vs}^0 \\ \mathbf{m}_{qp} - \mathbf{m}_{qp}^0 \\ \mathbf{m}_{qs} - \mathbf{m}_{qs}^0 \\ \mathbf{m}_{\rho} - \mathbf{m}_{\rho}^0 \end{bmatrix}. \quad (11)$$

We can focus on model residuals associated with one parameter class only, for instance the P-wave quality factor, by constructing model residual vectors where the four other contributions are replaced with zero vectors:

$$\mathbf{r}_{qp} = \begin{bmatrix} \mathbf{0} \\ \mathbf{0} \\ \mathbf{m}_{qp} - \mathbf{m}_{qp}^0 \\ \mathbf{0} \\ \mathbf{0} \end{bmatrix}, \quad (12)$$

or, going further, by setting all MN of the remaining non-zero elements, except the n th, to zero:

$$\mathbf{r}_{qp_n} = \begin{bmatrix} \mathbf{0} \\ \mathbf{0} \\ 0 \\ 0 \\ \vdots \\ m_{qp_n} - m_{qp_n}^0 \\ \vdots \\ 0 \\ \mathbf{0} \\ \mathbf{0} \end{bmatrix}. \quad (13)$$

Similar constructions, containing four zero vectors and one non-zero vector, allow us to form \mathbf{r}_A for any parameter type A of the five, or further, by setting all but the n th of those vector elements to zero, to form \mathbf{r}_{A_n} for any parameter type A or spatial position n of interest.

If the true subsurface model did not differ from the initial model in the n th element of parameter type A , then there would be no contribution from \mathbf{r}_{A_n} to the inversion. We can consider the case in which a given model residual \mathbf{r}_{A_n} does not exist by defining a model

$$\mathbf{m}'(\mathbf{r}_{A_n}) = \mathbf{m} - \mathbf{r}_{A_n}. \quad (14)$$

The result of the inversion

$$\hat{\mathbf{m}}'(\mathbf{r}_{A_n}) = \text{FWI}(\mathbf{d}(\mathbf{m}'(\mathbf{r}_{A_n}), \mathbf{m}^0)) \quad (15)$$

is then equal to $\hat{\mathbf{m}}$ less the contribution to the inversion from the model residual \mathbf{r}_{A_n} , implying that the contribution of \mathbf{r}_{A_n} to the inversion result is

$$\Delta\hat{\mathbf{m}}(\mathbf{r}_{A_n}) = \hat{\mathbf{m}} - \hat{\mathbf{m}}'(\mathbf{r}_{A_n}). \quad (16)$$

In so far as $\Delta\hat{\mathbf{m}}(\mathbf{r}_{A_n})$ represents changes in the model for variables other than the single non-zero element of \mathbf{r}_{A_n} , it represents cross-talk. Cross-talk contributions from a class of variables, rather than from a single variable, can be computed as $\Delta\hat{\mathbf{m}}(\mathbf{r}_A)$, where \mathbf{r}_A are the model residuals associated with a full class of parameters (as exemplified for the P-wave quality factor in equation 12). By including all of the variables describing parameter type A , the part of $\Delta\hat{\mathbf{m}}(\mathbf{r}_A)$ representing a change in variable B is a full measure of the cross-talk from A into B . In fact this framework allows the cross-talk from any set of FWI unknowns into any other set to be discussed quantitatively.

There are several advantages to using this approach to characterize cross-talk. It allows for the determination of cross-talk between any two sets of variables, not just those with the same position in space. This means that cross-talk between spatially separated variables can be identified. It offers the potential to study the effects of iteration on the inversion, a key consideration in FWI. It can also help to characterize the effectiveness of Hessian information in suppressing different modes of cross-talk, which can be very difficult to quantify using other approaches.

One may reasonably ask why we consider the contribution of an unknown parameter A , element n to the inversion to be the difference between the inversion result with and without \mathbf{r}_{A_n} , namely $\Delta\hat{\mathbf{m}}(\mathbf{r}_{A_n})$, rather than the result of an inversion involving model residual \mathbf{r}_{A_n} only. The key difference here is that the latter does not capture the interaction between \mathbf{r}_{A_n} and other model residuals. This distinction may be a fine one when analyzing some parameter classes, but when considering cross-talk from Q it can lead to a neglect of changes in the amplitude of other recovered anomalies. The definition of cross-talk we use here is able to include these effects.

NUMERICAL ANALYSIS OF VISCOELASTIC CROSS-TALK

We next discuss how to use the measure of cross-talk introduced above on a simple model, to allow for general conclusions to be drawn, in a way analogous to that in which radiation pattern analysis is used. Our main objectives are to (1) characterize the effects of acquisition geometry on cross-talk, to (2) identify the extent of cross-talk from quality factor variables into elastic variables at other positions, and to (3) investigate these behaviors for several optimization strategies. We calculate the cross-talk for a series of simulated problems, using the same model in each, but each time changing the acquisition geometry, optimization approach, or choice of \mathbf{r} .

Model geometry and inversion parameters

We designed a simple model with geometry selected to allow relatively general conclusions to be drawn about the character of viscoelastic parameter cross-talk. The design is not intended to represent geology, but rather to expose aspects of confusion between parameter values, especially those between quality factors and elastic properties which are separated in space. An unknown region of low Q (≈ 20) in both the P- and S-wave modes obscures from the sources and receivers a smaller region containing unknown changes in the elastic parameters (each a 10% increase over the initial model). The elastic region is a small circle at the center; the low Q_P and Q_S region is a larger circle containing it (Figure 1). The ini-

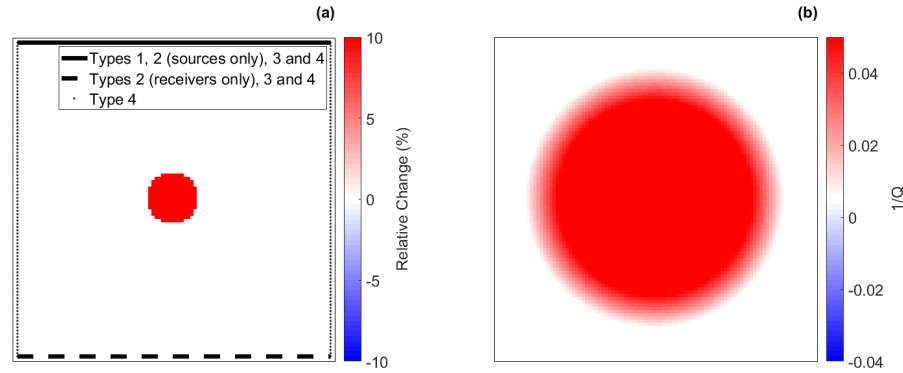


FIG. 1: The true model involves (a) elastic parameter unknowns confined to a small circular region at the center of the volume, and (b) P- and S-wave mode $1/Q$ unknowns occupying a larger and smooth circular region surrounding the smaller circle.

tial model used in the inversion is constant for each parameter, set equal to the background values. The attenuative region is chosen to produce a high probability of cross-talk between Q_P or Q_S variables that obscure elastic perturbations from source/receiver positions. Because of the differences in the relative magnitudes of the model errors between the quality factor and other parameters, these tests should not be interpreted as providing strong evidence for the relative amplitude of cross-talk from quality factor variables as compared to elastic variables. Cross-talk from Q_P to v_P can be directly compared with Q_S to v_P or Q_S to ρ , for instance, but caution should be used when considering comparisons of cross-talk terms arising from different relative residuals, e.g. Q_P to v_P and ρ to v_P .

In the analysis, cross talk from seven different choices of model residual is considered. In five of these, the residual is chosen to be the full vector of unknowns for each parameter type (i.e., \mathbf{r}_A for parameter A in the terminology of the previous section). These allow for calculation of the total cross-talk from and to each parameter in the inversion. We refer to the cross-talk from the parameter $\alpha_2 v_P^{-2}$ as ‘cross-talk from v_P ’, and adopt similar terminology for the other parameters. In the other two cases, the residual vector is chosen to include only some of several parameter types, namely, the outer rings of the Q_P and Q_S anomalies, as shown in Figure 2 (i.e., \mathbf{r}_{A_n} for values of n corresponding to designated regions of space). These are chosen so that we can develop an understanding of cross-talk between the obscuring Q_P and Q_S region and the elastic anomaly, an important example of cross-talk between spatially distant variables. Instances of cross-talk from the partial (outer ring) model residuals shown in Figure 2, for $1/Q_P$ and $1/Q_S$, are referred to as cross-talk from primed variables Q'_P and Q'_S .

We consider four acquisition geometries, each with sources and receivers evenly spaced along one or several edges of the model in Figure 1. In Type 1, sources and receivers are placed along the top of the model, and reflections are the main source of information. In Type 2, sources are placed at the top of the model and receivers on the bottom, simulating a transmission or cross-well geometry. In Type 3, sources/receivers are placed on both the top and bottom of the model, providing comprehensive reflection and transmission information. In Type 4, to examine fundamental features of cross-talk, sources/receivers are placed on

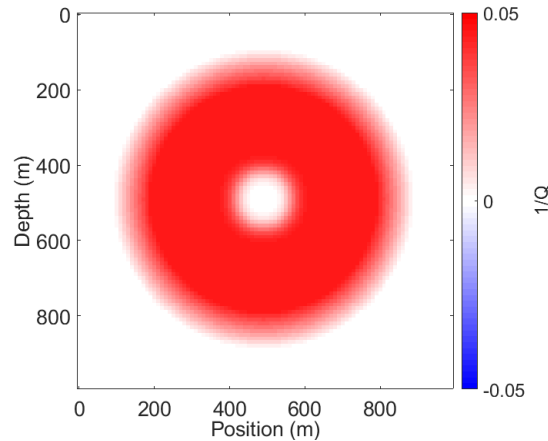


FIG. 2: Model residual used to calculate cross-talk from Q'_P and Q'_S

all four sides. These acquisition geometries were chosen to help develop an understanding of the relative importance of reflection and transmission ray-paths in the resolution of the parameters. Explosive sources are considered, and both components of displacement are recorded at the receivers. These cases are chosen to determine the importance of reflection and transmission ray-paths on the different cross-talk modes, and to compare with cross-talk in the case of ideal acquisition.

In each inversion test, 10 frequency bands are inverted, each containing 5 evenly-spaced frequency values. The upper end of the bands is increased with iteration, the first spanning 1-2Hz, and the last 1-20Hz. No regularization is used, except in the examples involving truncated Gauss-Newton optimization, where a small stabilization term is added to the Hessian matrix. Three different numerical optimization strategies are considered.

Cross-talk within single-iteration steepest-descent updating

In our first set of numerical tests, we consider an FWI implementation which employs only a single iteration of steepest descent optimization at each frequency band. With ten frequency bands this results in ten total iterations. This set-up allows us to examine the cross-talk behavior with limited impact from the iterative nature of the inversion problem. This is the type of cross-talk that radiation pattern analysis is best suited to describe.

Figure 3 illustrates the cross-talk into the inversion parameter $\alpha_2 v_P^{-2}$, in terms of the equivalent relative change in v_P , referred to here as ‘cross-talk into v_P ’. This figure is subdivided into several panels, each of which illustrate the cross-talk into v_P from one of the model residual terms, given data from one of the acquisition geometries considered. Within each panel the x dimension and z dimension represent x and z position. The amplitudes of the model changes $\Delta \hat{\mathbf{m}} = \hat{\mathbf{m}} - \hat{\mathbf{m}}_0$ differ considerably for the different acquisitions. To allow for comparison, the cross-talk amplitudes were normalized so as to be fractions of the largest amplitude in the model change $\Delta \mathbf{m}$ calculated for that acquisition type.

In Figure 3 we observe strong leakage from Q_P into v_P , as expected given the mathe-

matically similar roles played by the two parameters in equations 4 and 3. Cross-talk into v_P from all others is substantial in the Type 1 acquisition; cross-talk from v_S to v_P remains high in the other acquisition types. The cross-talk term from Q_P into v_P for acquisition type 4 is particularly notable. As the Q_P anomaly is largely homogeneous in the interior region, cross talk into v_P from Q_P at or near the same point might be expected to also be homogeneous inside of the region where the Q_P anomaly is present. Instead, significantly larger amplitude cross-talk can be observed in a small interior region, approximately where the v_P anomaly is present. This suggests that an additional cross-talk mechanism must be present in this specific area. A likely cause is that the obscuring Q_P region is coupled with, and confuses, the spatially distant v_P anomaly. This can be verified by examining the cross-talk between the outer Q_P region alone and v_P , i.e., the cross-talk from Q'_P .

Still within Figure 3, we observe in the Type 4 acquisition similar cross-talk from Q_P and Q'_P , including for the interior region. This suggests that cross-talk from the obscuring Q_P region is not only present at the center of the model, it is in fact dominant in this case. Comparison of the cross-talk from Q_P and Q'_P for the other acquisition types shows similar behavior; the obscuring Q region contributes substantially to the cross-talk at the center of the model. While the relative amplitude of cross-talk from Q_S is smaller, Figure 3 exhibits similar trends in those cross-talk terms.

The corresponding cross-talk signatures into density and v_S are plotted in Figures 5 and 6. The Q -to-density terms are notable as most of the observed cross-talk occurs between spatially separated variables at the location of the density anomaly; relatively little cross-talk between co-located variables can be observed here. The cross-talk into density in the Type 2 acquisition is very strong, but this is consistent with expectations based on purely elastic results (it is well established that density is very difficult to recover from transmission data). Cross-talk into v_S again involves confusing between spatially-separated variables. Significant contributions come from both Q_P and Q_S in this case.

The cross-talk into Q_P and Q_S are plotted in Figures 4 and 7. The most striking feature is the low degree of cross-talk *from* the elastic anomalies *into* an obscuring Q region, despite the fact that the reverse is observed for all three elastic parameters. Both of these variables exhibit strong cross-talk with their corresponding velocities for each acquisition type. The cross-talk from Q_S to Q_P for acquisition Type 4 is notable for the fact that, in this one case, cross-talk from the obscuring region into the center of the model appears to be negligible. The cross-talk from Q'_S in this case is very similar to the model residual considered in that case (Figure 2), suggesting that cross-talk from co-located unknowns dominates here.

Cross-talk within multiple-iteration steepest-descent updating

While the measures shown in the previous subsection are informative about the cross-talk in the gradient, there are limits to the insight they provide about the actual experience of solving the FWI problem, in which iteration plays an important role. To better understand the impact of iteration we consider in this section steepest descent optimization with five iterations per frequency band (i.e., involving a total of 50 iterations).

In Figure 8 the cross-talk into v_P using an iterative steepest-descent optimization is

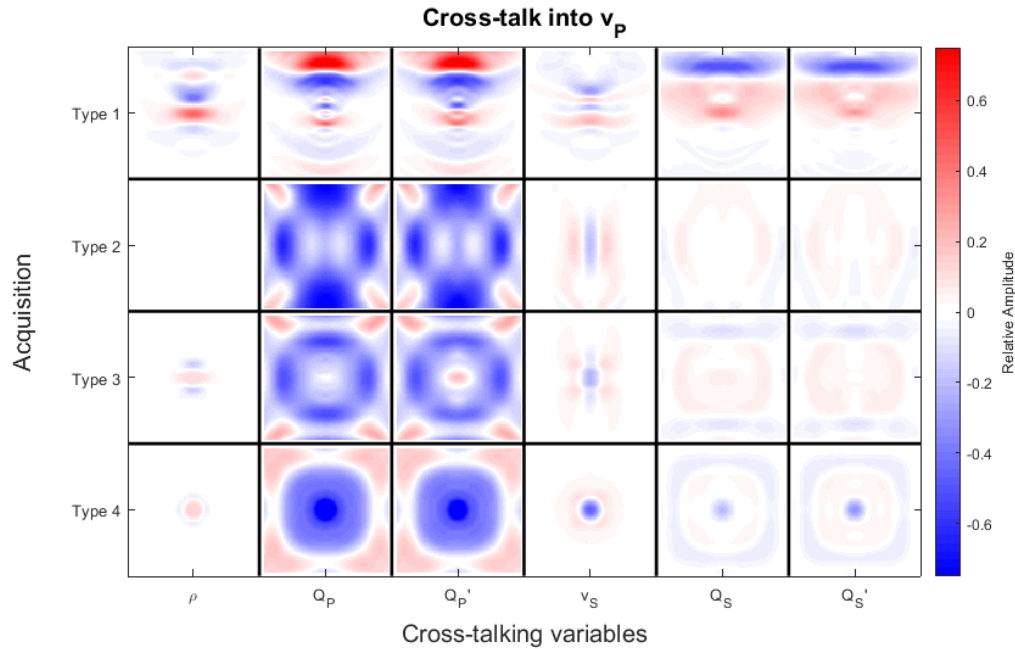


FIG. 3: Numerically calculated cross-talk into v_P with one iteration of steepest-descent optimization per frequency band.

plotted. Comparison with Figure 3 reveals similarities but also contrasts with the single-iteration case. While cross talk from the attenuation variables in acquisition geometries including transmission ray-paths (Types 2-4) is substantially suppressed by iteration, cross-talk in the Type 1 reflection-only acquisition is minimally improved, as is the cross-talk from density and v_S . The differences between cross talk signatures after a small (Figure 3) and large (Figure 8) number of iterations are substantial for several acquisition geometries; the effects of iteration on cross-talk appear to be significant here.

Cross-talk into density with this optimization approach, plotted in Figure 10, behaves similarly: cross-talk is notably suppressed in some panels, but not in others. In comparison with Figure 5, cross-talk from Q_S is evidently reduced in the region of the elastic anomalies in both acquisition Type 1 (reflection) and 4 (surrounding). Similar reduction occurs for the cross-talk from Q_P for acquisition Type 4. As with cross-talk into v_P , there is limited reduction in cross-talk from elastic parameters.

Cross-talk into v_S is substantially reduced from all other parameters in this approach, especially in the cross-talk from Q_P (Figure 11 as compared to Figure 6). The reductions are also largely limited to acquisition geometries other than type 1. Cross-talk into Q_S undergoes similar reductions (figures 12 and 7). The similar behavior of these two parameters in contrast to the others is likely due to the great importance of converted waves on the recovery of these parameters in comparison to the other variables. If non-explosive sources were considered, these results might be expected to change.

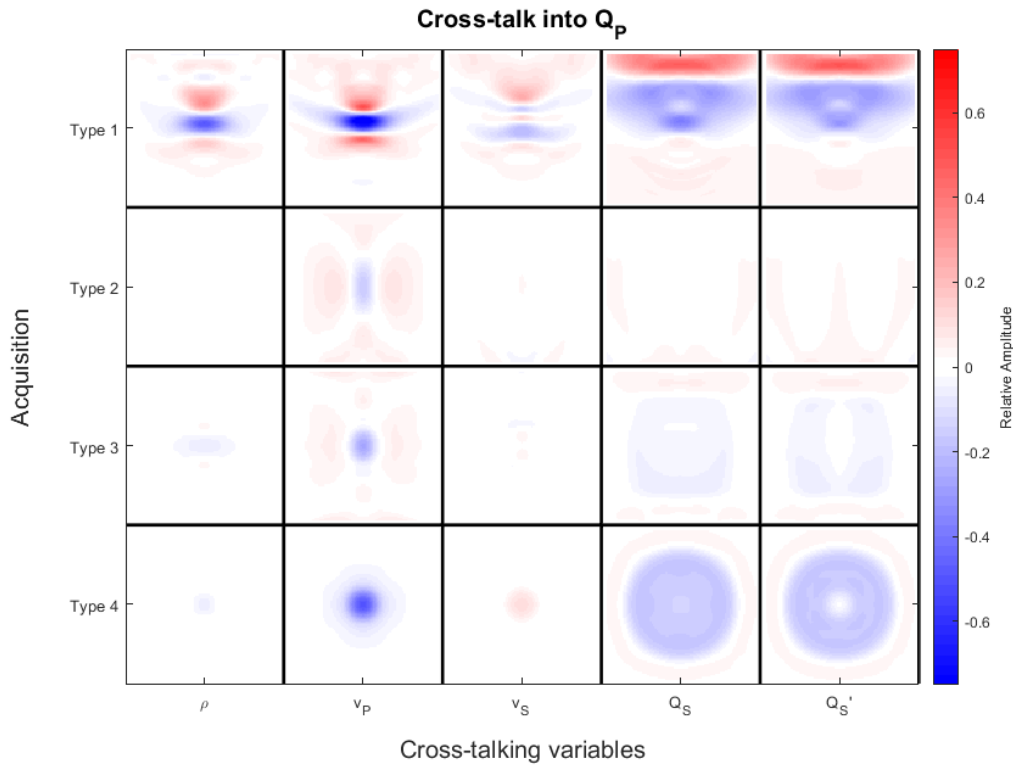


FIG. 4: Numerically calculated cross-talk into Q_P with one iteration of steepest-descent optimization per frequency band.

Cross-talk into Q_P from v_S and Q_S is reduced through iteration, as is cross-talk from v_P in acquisition Type 4, in which sources and receivers surround the unknown structures (Figure 9). In this case, however, cross-talk appears to increase slightly for several parameters in the Type 2 acquisition tests.

Cross-talk within Truncated Gauss-Newton updating

The Hessian matrix is known to play a major role in the suppression of cross-talk. In this subsection we investigate cross-talk in the context of truncated Gauss-Newton optimization, where the Gauss-Newton step is iteratively estimated (e.g. Metivier et al., 2013). Five inner-loop iterations were used at each FWI iteration to calculate the approximation to the Gauss-Newton step.

The cross-talk results calculated from these FWI updates are plotted in Figures 13–17. These results are similar to those obtained using steepest descent with five iterations per frequency band. This suggests that at the cost level chosen (i.e., with a small number of truncated-Newton iterations) there are only small differences between these approaches. An exception to this similarity is evident for cross-talk into v_S , as plotted in Figure 16. Cross-talk from Q_P is substantially reduced in this case, and cross-talk from Q_S somewhat reduced, except for acquisition Type 1.

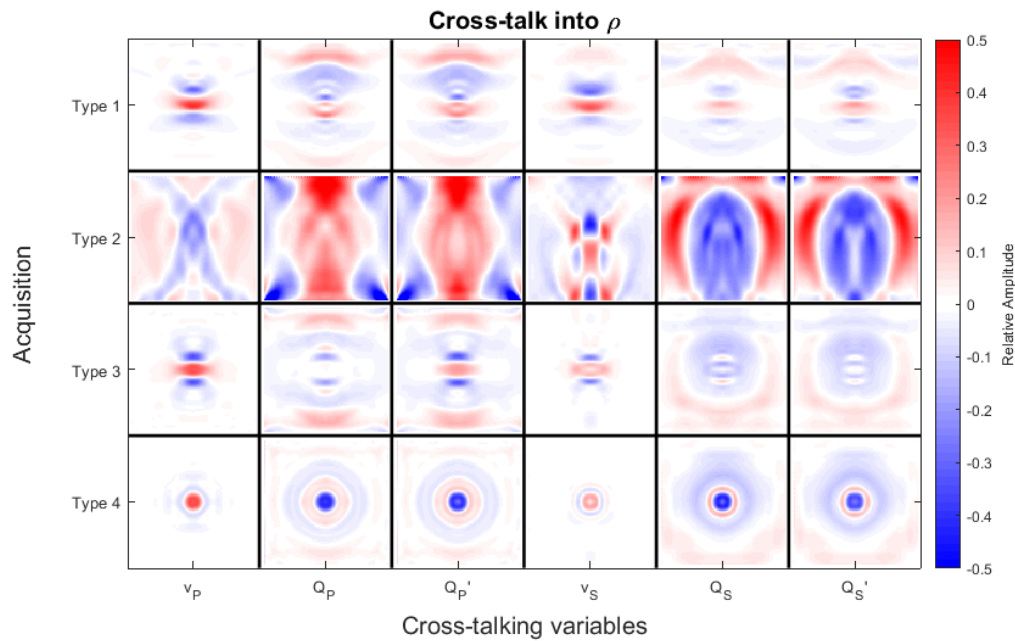


FIG. 5: Numerically calculated cross-talk into ρ with one iteration of steepest-descent optimization per frequency band.

DISCUSSION

The numerical calculations of the cross-talk quantities introduced in this paper appear to be informative about the various modes of cross-talk present in viscoelastic FWI; a key next step is to implement viscoelastic FWI based on this information to reduce cross-talk. Radiation patterns are often used in elastic FWI to guide strategies for cross-talk reduction based on scattering angles. In many of these approaches, data from angle ranges within which only one parameter has a significant radiation energy are used to update just these parameters. If such ranges do not exist, alternate parameterizations may be sought. This is difficult to apply when considering attenuation, because velocity and Q radiation patterns are not made distinct by scattering angle information (Keating and Innanen, 2017).

If cross-talk cannot be limited simply through data-selection strategies, the second derivative information contained in the Hessian must play a major role in a successful cross-talk reduction scheme. The technique we have described here is expected to be a useful means of comparing the efficacy of cross-talk reduction between optimization strategies using different approaches to approximating the effect of the Hessian matrix.

CONCLUSIONS

Inter-parameter cross-talk in full waveform inversion is often characterized through the use of radiation patterns. These are poorly suited for viscoelastic FWI because of the significant potential for cross-talk between variables distant from one another in space,

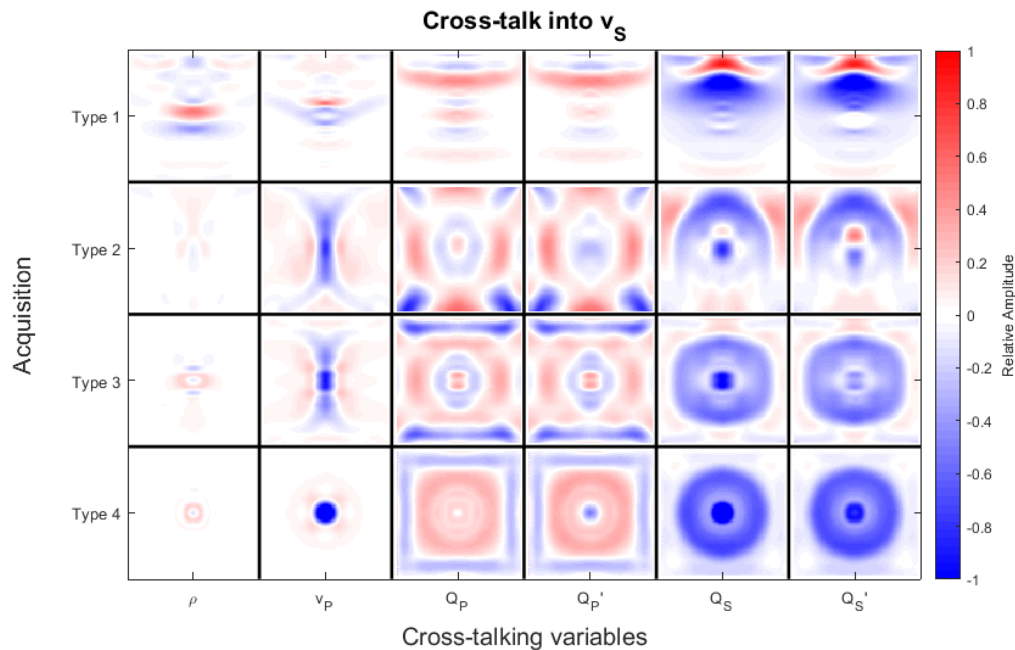


FIG. 6: Numerically calculated cross-talk into v_S with one iteration of steepest-descent optimization per frequency band.

and the challenge of interpreting the frequency and phase dependence of radiation patterns on cross-talk. Simple numerical simulations offer an alternate approach for characterizing cross-talk which may be better suited to the viscoelastic problem. Tests using this approach suggest that cross-talk between velocity variables and the corresponding Q variables is quite strong, and occurs both between variables at the same location and those far apart. Cross-talk between spatially separated variables can be the dominant contribution at a given point in space. Iteration and Hessian information have a major impact on cross-talk, and this approach offers a means of capturing this dependence.

ACKNOWLEDGEMENTS

This work was funded by CREWES industrial sponsors and NSERC (Natural Science and Engineering Research Council of Canada) through the grant CRDPJ 461179-13. S. Keating was also supported by the Earl D. and Reba C. Griffin Memorial Scholarship.

REFERENCES

- Alkhalifah, T., and Plessix, R., 2014, A recipe for practical full-waveform inversion in anisotropic media: An analytical parameter resolution study: *Geophysics*, **79**, R91–R101.
- Berenger, J., 1994, A perfectly matched layer for the absorption of electromagnetic waves: *Journal of computational physics*, **114**, 185–200.
- Futterman, W. I., 1962, Dispersive body waves: *Journal of Geophysical Research*, **67**, 5279–5291.

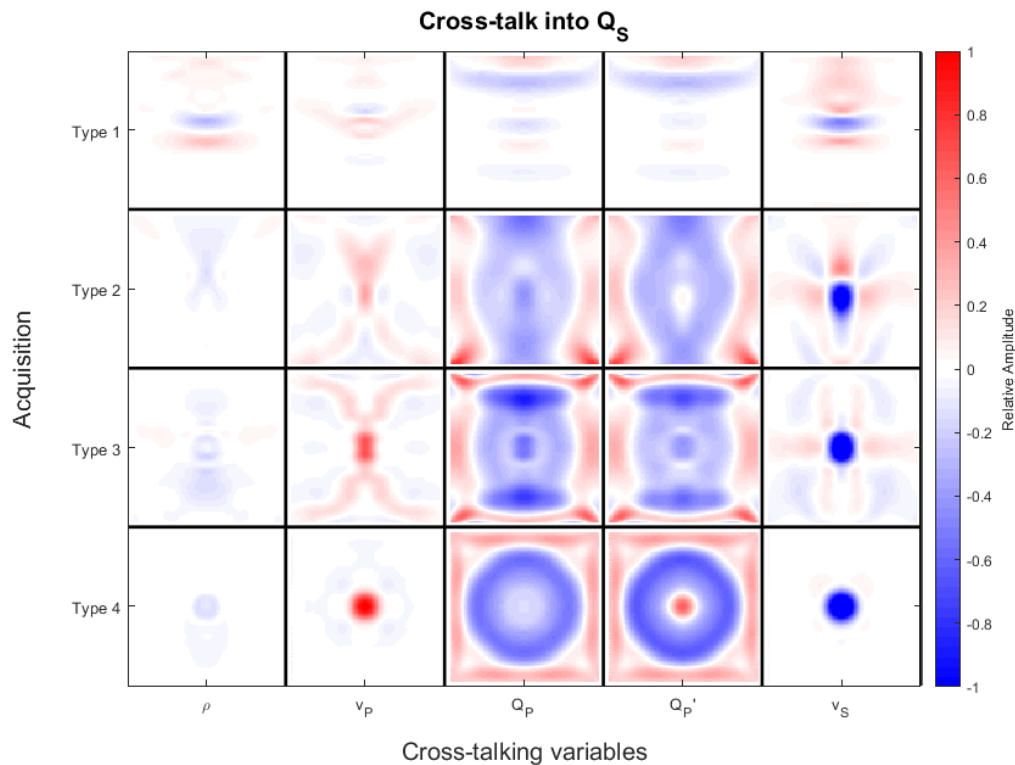


FIG. 7: Numerically calculated cross-talk into Q_S with one iteration of steepest-descent optimization per frequency band.

Hak, B., and Mulder, W., 2011, Seismic attenuation imaging with causality: *Geophysical Journal International*, **184**, 439–451.

Hicks, G., and Pratt, R., 2001, Reflection waveform inversion using local descent methods: Estimating attenuation and velocity over a gas-sand deposit: *Geophysics*, **66**, 598–612.

Innanen, K. A., and Weglein, A. B., 2007, On the construction of an absorptive-dispersive medium model via direct linear inversion of reflected seismic primaries: *Inverse Problems*, **23**, 2289–2310.

Kamath, N., Tsvankin, I., and Díaz, E., 2017, Elastic full-waveform inversion for vti media: A synthetic parameterization study: *Geophysics*, **82**, No. 5, C163–C174.

Kamei, R., and Pratt, R., 2013, Inversion strategies for visco-acoustic waveform inversion: *Geophysical Journal International*, **194**, 859–884.

Keating, S., and Innanen, K. A., 2017, Cross-talk and frequency bands in truncated newton an-acoustic full waveform inversion: *SEG Expanded Abstracts*.

Keating, S., Li, J., and Innanen, K. A., 2018, Viscoelastic fwi: solving for q_p , q_s , v_p , v_s , and density: *CREWES Annual Report*, **30**.

Köhn, D., De Nil, D., Kurzmann, A., Przebindowska, A., and Bohlen, T., 2012, On the influence of model parametrization in elastic full waveform tomography: *Geophysical Journal International*, **191**, No. 1, 325–345.

Kolsky, H., 1956, The propagation of stress pulses in viscoelastic solids: *Philosophical Magazine*, **1**, 693–710.

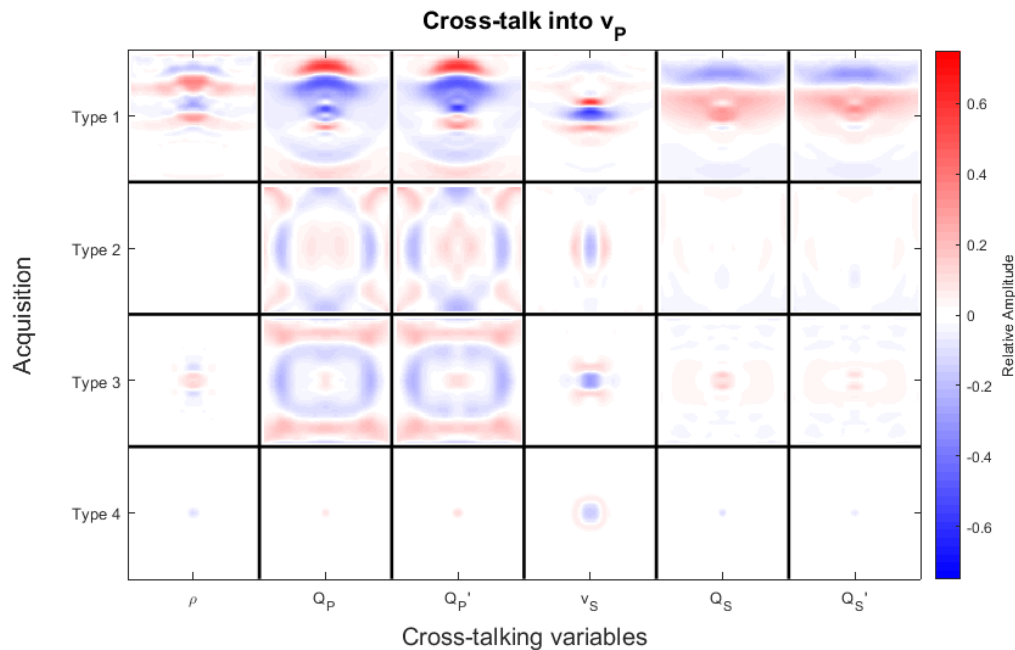


FIG. 8: Numerically calculated cross-talk into v_P with five iterations of steepest-descent optimization per frequency band. Compare with figure 3.

Malinowski, M., Operto, S., and Ribodetti, A., 2011, High-resolution seismic attenuation imaging from wide-aperture onshore data by visco-acoustic frequency-domain full-waveform inversion: *Geophysical Journal International*, **186**, 1179–1204.

Métivier, L., Brossier, R., Operto, S., and Virieux, J., 2015, Acoustic multi-parameter FWI for the reconstruction of P-wave velocity, density and attenuation: preconditioned truncated Newton approach: *SEG Expanded Abstracts*, 1198–1203.

Metivier, L., Brossier, R., Virieux, J., and Operto, S., 2013, Full waveform inversion and the truncated newton method: *Siam J. Sci. Comput.*, **35**, B401–B437.

Moradi, S., and Innanen, K., 2016, Scattering of homogeneous and inhomogeneous seismic waves in low-loss viscoelastic media: *Geophys. J. Int.*, **202**, 1722–1732.

Oh, J., and Alkhalifah, T., 2016, The scattering potential of partial derivative wavefields in 3-d elastic orthorhombic media: an inversion prospective: *Geophys. J. Int.*, **206**, 1740–1760.

Operto, S., Gholami, Y., Prieux, V., Ribodetti, A., Brossier, R., Metivier, L., and Virieux, J., 2013, A guided tour of multiparameter full-waveform inversion with multicomponent data: From theory to practice: *The Leading Edge*, 1040–1054.

Pan, W., Geng, Y., and Innanen, K. A., 2016, Estimation of elastic constants for hti media using gauss-newton and full-newton multiparameter full-waveform inversion: *Geophysics*, **81**, R275–R291.

Pan, W., Geng, Y., and Innanen, K. A., 2018, Interparameter trade-off quantification and reduction in isotropic-elastic full-waveform inversion: synthetic experiments and hussar land data set application: *Geophys. J. Int.*, **213**, 1305–1333.

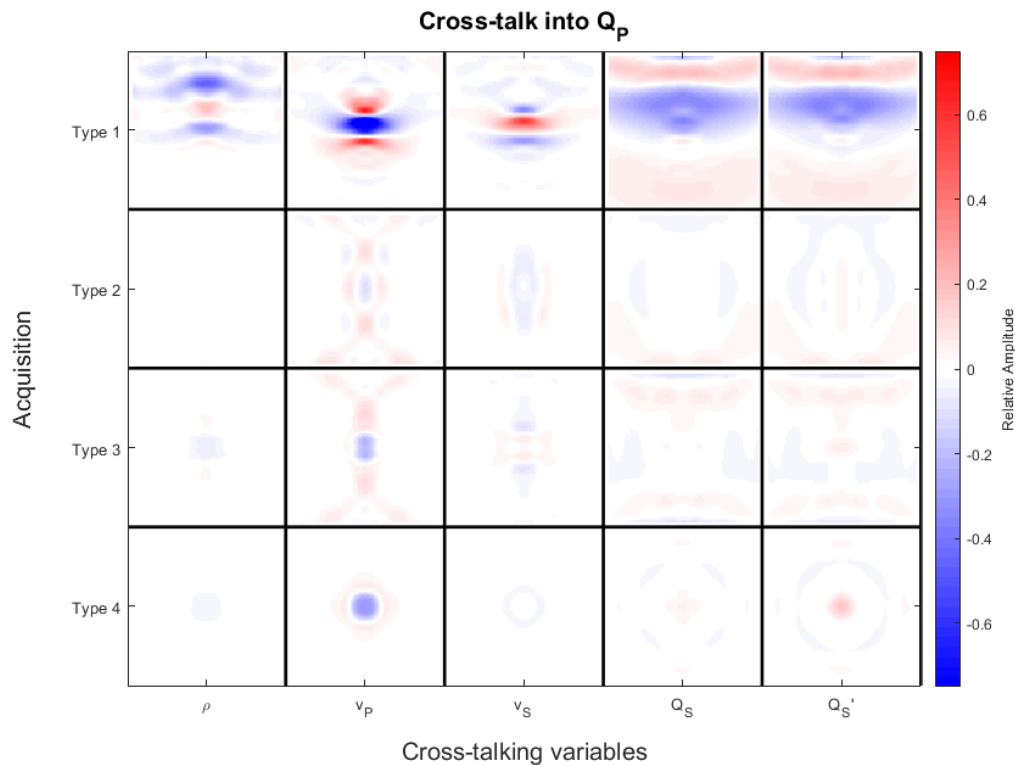


FIG. 9: Numerically calculated cross-talk into Q_P with five iterations of steepest-descent optimization per frequency band. Compare with figure 4.

Plessix, R. E., Stopin, A., Kuehl, H., Goh, V., and Overgaag, K., 2016, Visco-acoustic full waveform inversion: EAGE Expanded Abstracts.

Pratt, R., 1990, Frequency-domain elastic wave modeling by finite differences: A tool for crosshole seismic imaging: *Geophys. J. Int.*, **133**, 341–362.

Tarantola, A., 1984, Inversion of seismic reflection data in the acoustic approximation: *Geophysics*, **49**, 1259–1266.

Tarantola, A., 1986, A strategy for nonlinear inversion of seismic reflection data: *Geophysics*, **51**, 1893–1903.

Tromp, J., Tape, C., and Liu, Q., 2005, Seismic tomography, adjoint methods, time reversal and banana-doughnut kernels: *Geophysical Journal International*, **160**, No. 1, 195–216.

Virieux, J., and Operto, S., 2009, An overview of full-waveform inversion in exploration geophysics: *Geophysics*, **74**, No. 6, WCC1.

Yang, P., Brossier, R., Métivier, L., and Virieux, J., 2016, A review on the systematic formulation of 3-d multiparameter full waveform inversion in viscoelastic medium: *Geophysical Journal International*, **207**, No. 1, 129–149.

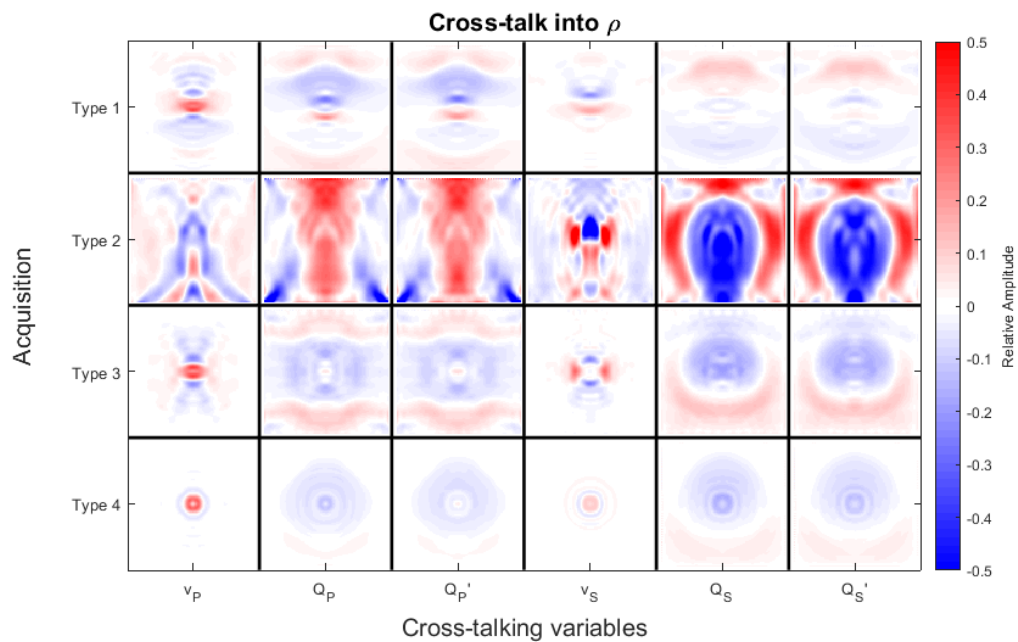


FIG. 10: Numerically calculated cross-talk into ρ with five iterations of steepest-descent optimization per frequency band. Compare with figure 5.

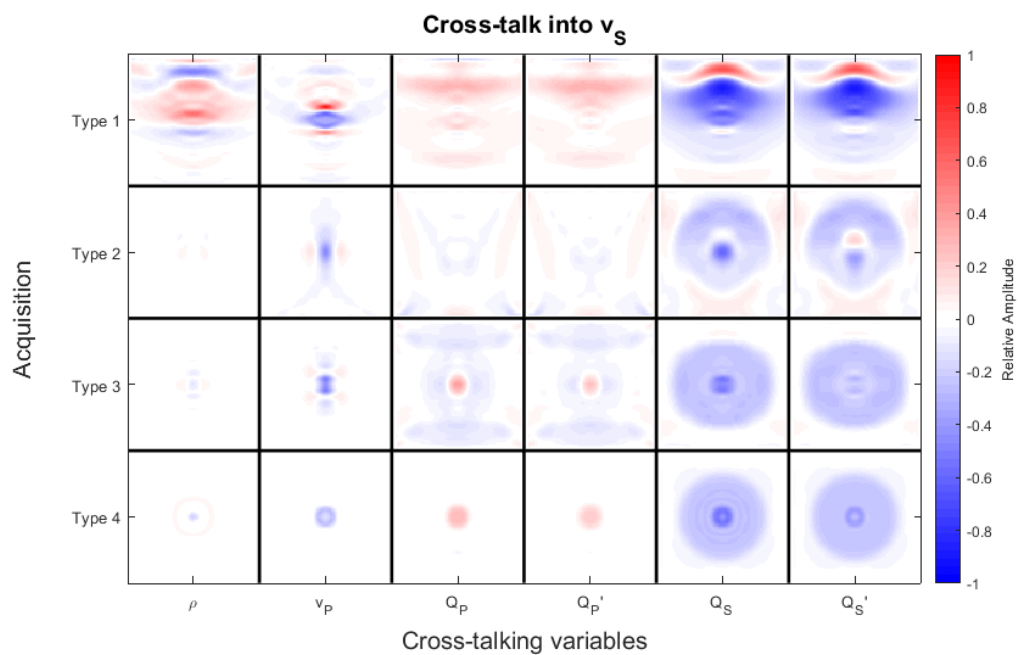


FIG. 11: Numerically calculated cross-talk into v_s with five iterations of steepest-descent optimization per frequency band. Compare with figure 6.

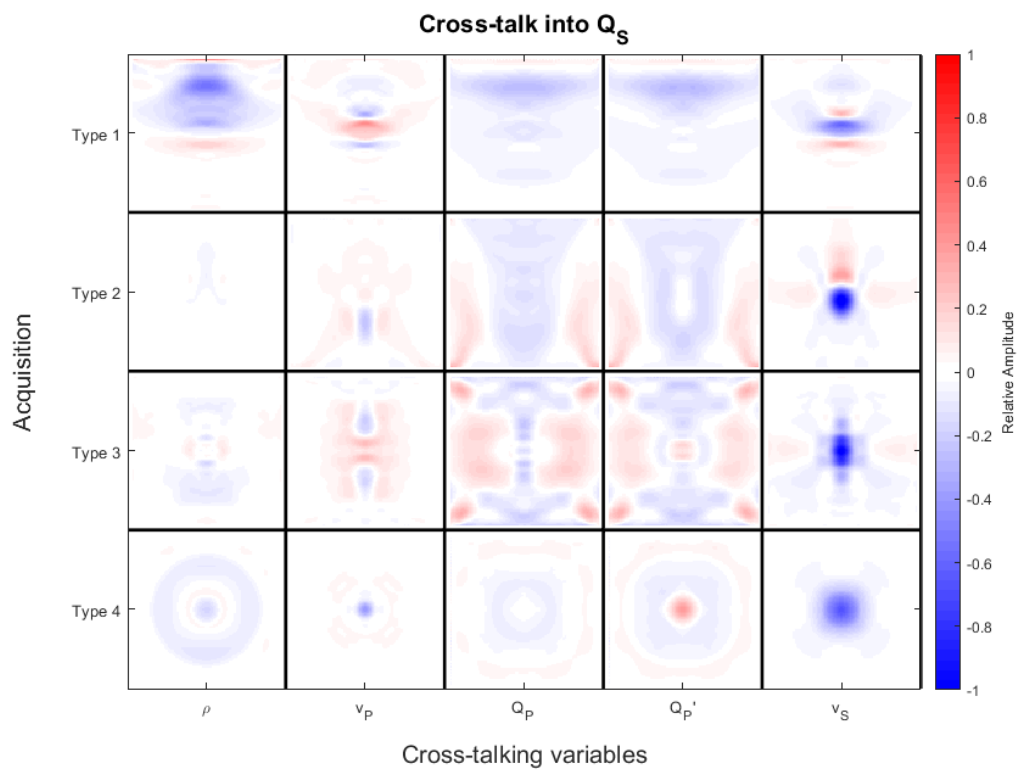


FIG. 12: Numerically calculated cross-talk into Q_S with five iterations of steepest-descent optimization per frequency band. Compare with figure 7.

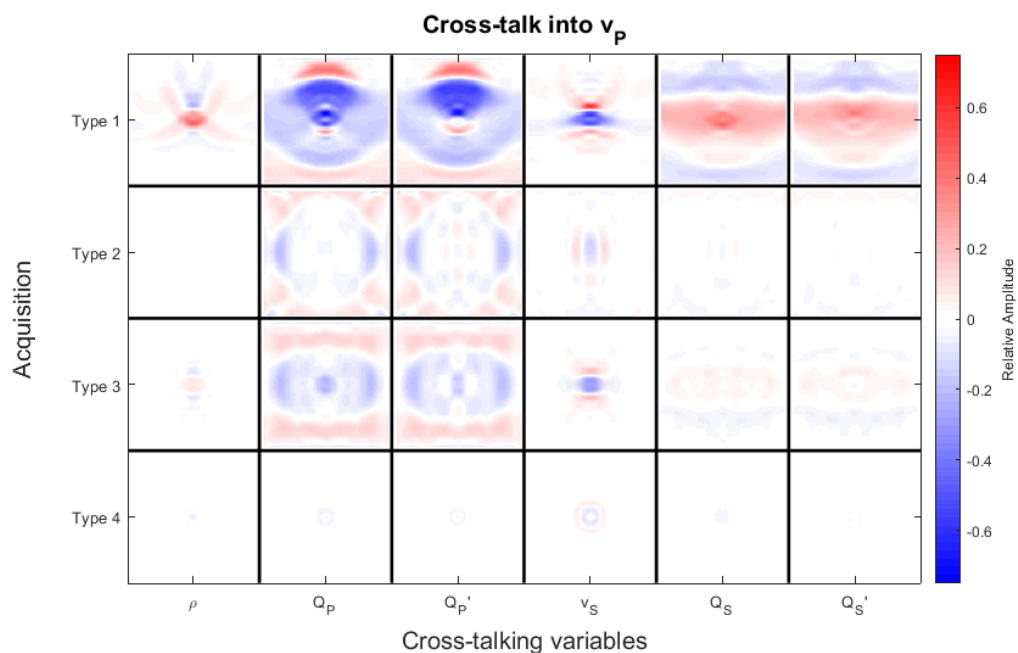


FIG. 13: Numerically calculated cross-talk into v_p with truncated Gauss-Newton optimization. Compare with figures 3 and 8.

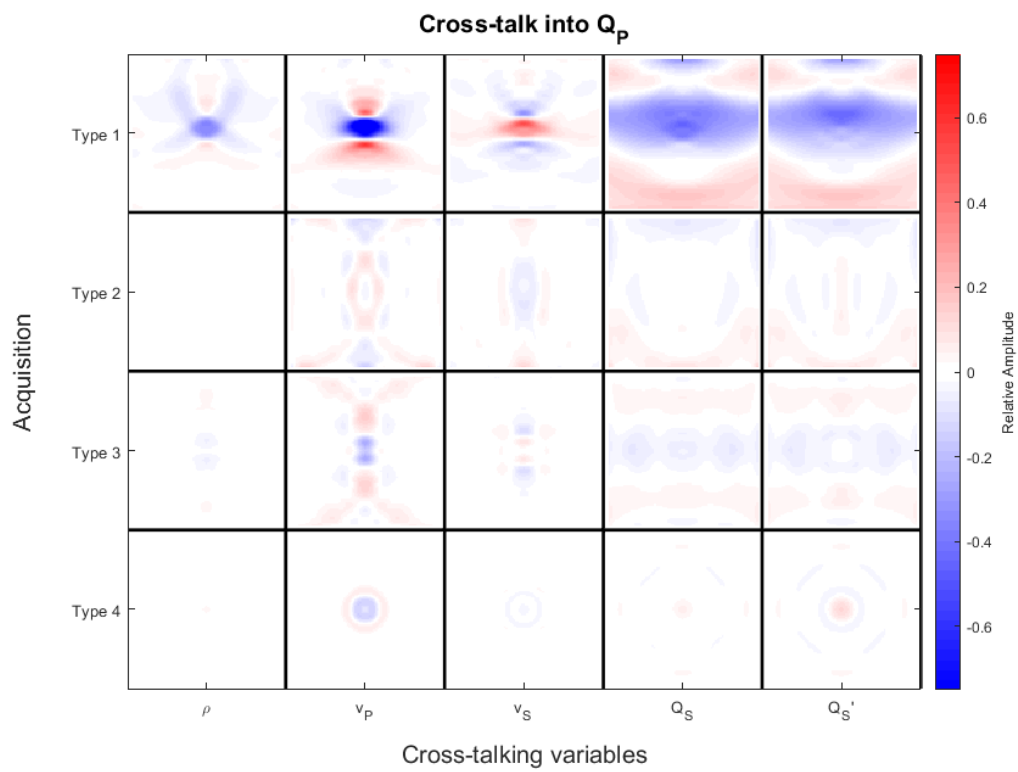


FIG. 14: Numerically calculated cross-talk into Q_p with truncated Gauss-Newton optimization. Compare with figures 4 and 9.

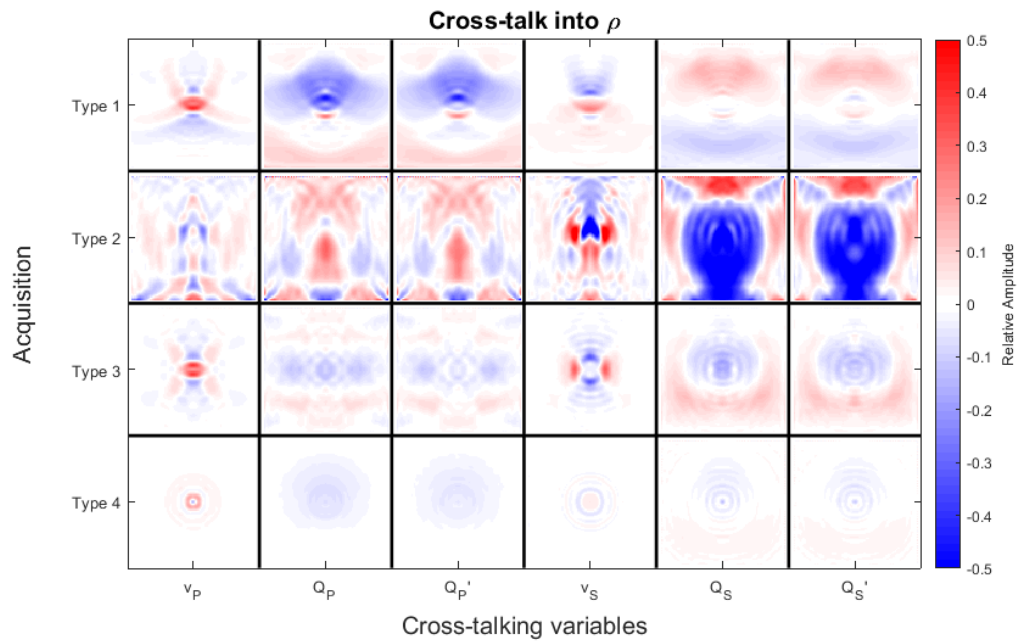


FIG. 15: Numerically calculated cross-talk into ρ with truncated Gauss-Newton optimization. Compare with figures 5 and 10.

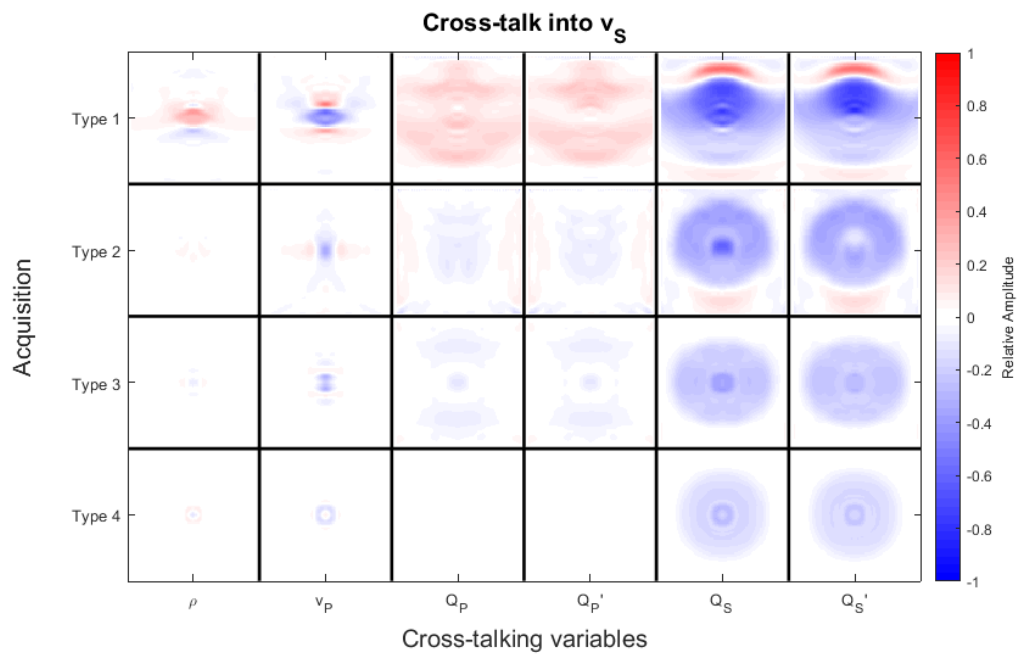


FIG. 16: Numerically calculated cross-talk into v_s with truncated Gauss-Newton optimization. Compare with figures 6 and 11.

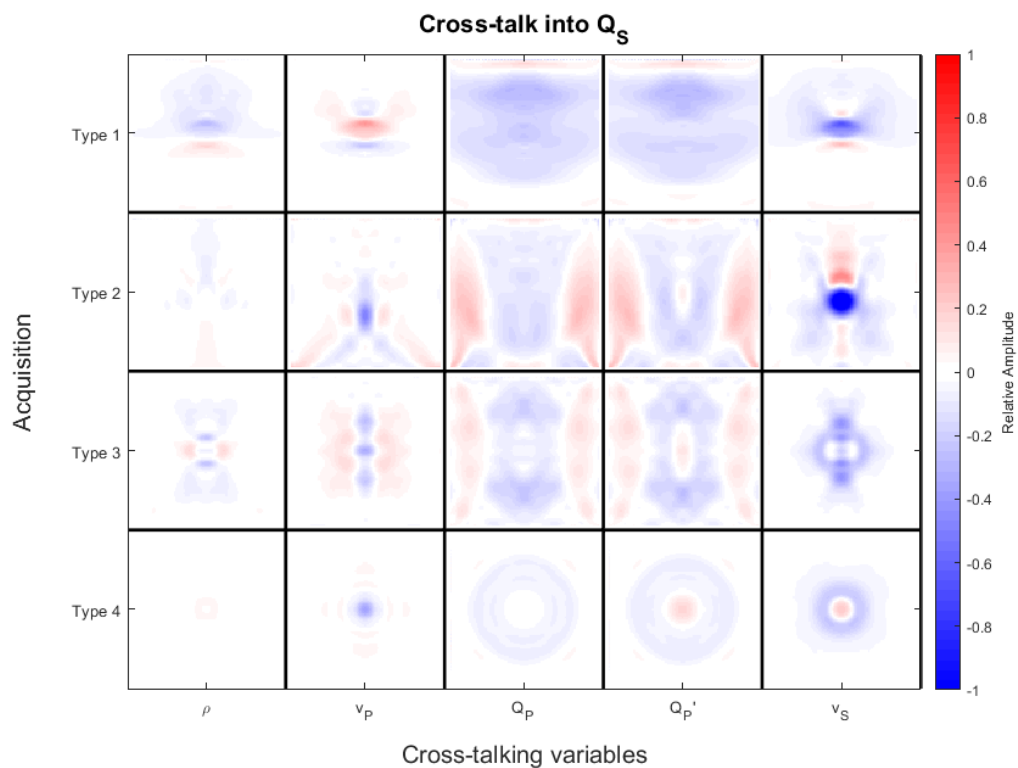


FIG. 17: Numerically calculated cross-talk into Q_S with truncated Gauss-Newton optimization. Compare with figures 7 and 12.